Pergamon

0042-6989(94)00189-8

Vision Res. Vol. 35, No. 11, pp. 1585–1594, 1995

0042-6989/95 $9.50+0.00

Adaptation Mechanisms in Spatial Vision—I. Bleaches and Backgrounds

LANCE W. HAHN,*† WILSON S. GEISLER*‡

Received 21 April 1994; in revised form 8 August 1994

To examine how the mechanisms of bleaching and background adaptation affect spatial pattern vision, contrast detection thresholds were measured in the fovea for sinusoidal (increment-Gabor) targets, during long-term dark adaptation following full bleaches, and against steady adapting backgrounds of various intensities. The dark-adaptation curves were found to be invariant in shape over the range of spatial frequencies tested (1–15 c/deg); in other words, the amplitude sensitivity functions were invariant during dark adaptation. These results support the hypothesis that bleaching adaptation is local and multiplicative. On the other hand, the background-adaptation curves measured for different spatial frequencies were found to converge as background intensity increased; the amplitude sensitivity functions became flatter. These results reject the equivalent-background hypothesis.

Dark adaptation Light adaptation Spatial-frequency channels Increment-Gabor Bleaching

INTRODUCTION

Most of the spatial pattern information available in the environment is the result of relatively subtle differences in surface reflectance. To detect these reflectance variations the visual system must maintain a high sensitivity to small differences in retinal illumination, and hence a high response gain in its visual neurons. Unfortunately, ambient illumination levels in the environment vary over many orders of magnitude, while biophysical limitations necessarily leave neurons with a rather small dynamic range. The visual system solves this mismatch between the range of ambient light levels and the dynamic range of neurons by employing a variety of adaptation mechanisms (for reviews see, for example, Shapley and Enroth-Cugell, 1984; Hood & Finkelstein, 1986; Walraven, Enroth-Cugell, Hood, MacLeod & Schnapf, 1990). Without these adaptation mechanisms, the ability to detect and discriminate spatial patterns would be greatly degraded.

The most important and complex adaptation mechanisms are those in the retina which adjust the dynamic range of visual neurons to match the ambient light level. There is considerable psychophysical and physiological evidence for two main classes of retinal adaptation mechanism: multiplicative mechanisms, which (in effect) scale input levels by a multiplicative factor, and subtractive mechanisms, which (in effect) subtract a factor from the input levels.

*Center for Vision and Image Sciences, University of Texas at Austin, Mezes Hall, 330, Austin, TX 78712, U.S.A.
†Present address: Department of Neuroscience, University of Pennsylvania
‡To whom all correspondence should be addressed.

A number of recent studies have been directed at understanding the spatial properties of these retinal adaptation mechanisms (Cicerone, Hayhoe & MacLeod, 1990; Hayhoe, 1990; Hayhoe & Smith, 1989); however, few have been directed at the question of how the adaptation mechanisms contribute to general spatial pattern vision. This paper and the next (Kortum & Geisler, 1995) report measurements of spatial pattern detection thresholds for sinewave grating targets, as a function of spatial frequency, under a variety of light- and dark-adaptation conditions.

Bleaching adaptation

Although adaptation mechanisms can be roughly divided into the categories of multiplicative and subtractive, there appear to be two or more mechanisms within these categories, each with a different time constant (and perhaps other unique properties as well). The mechanisms with long time constants (the *long-term adaptation mechanisms*) traditionally have been isolated in dark-adaptation experiments, where the eye is initially exposed to an intense background level (a *bleaching field*) and sensitivity is measured as a function of time after the offset of the background. Such experiments show that following exposure to an intense bleaching field, the dynamic range of the cone system takes up to 10–12 min to return to its dark-adapted level. (Recovery in the rod system is, of course, even slower.)

Geisler (1981) used a flashed-background paradigm (Geisler, 1978b; Hood, Ilves, Mauer, Wandell & Buckingham, 1978) to measure the type and strength of adaptation mechanisms operating during long-term dark adaptation in the cone system. In this paradigm,

increment threshold functions for small probes on flashed backgrounds (probe-flash curves) are measured under different states of adaptation—in the case of bleaching adaptation, at different points in time during dark adaptation. The shape of a probe-flash curve serves as a signature of the type and strength of the adaptation mechanism; each type of mechanism produces a unique effect on the shape (e.g. see Geisler, 1983). Multiplicative adaptation affects the entire probe-flash curve (shifting it up and to the right along a 45° line), whereas subtractive adaptation primarily affects the curve at low flash intensities. Geisler's (1981) dark-adaptation data indicate that multiplicative adaptation accounts for essentially all of the changes in the probe-flash curves during the course of long-term dark adaptation (1–10 min) in the cone system.

Several investigators have attempted to measure the spatial spread of bleaching adaptation in the cone system. Brindley (1962) asked subjects to report on the appearance of long-term afterimages produced by brief, intense presentations (to the fovea) of square-wave grating patterns. The subjects reported that the afterimages became progressively more blurred in appearance during dark adaptation, indicating a substantial spread of the adaptation effects. However, recent replications using very brief (50 msec) exposures (Cicerone *et al.*, 1990; MacLeod & Hayhoe, 1976) found no evidence for blurring, suggesting that eye movements may have been responsible for Brindley's results. Cicerone *et al.* (1990) also used a more objective method (based upon the method that Rushton and Westheimer (1962) used to measure the spread of adaptation in rods), and found further evidence for very localized adaptation in the cone system. The spread of adaptation they observed was on the order of the diameter of a single cone photoreceptor (after correction for the effects of optical blur).

If, in fact, the long-term adaptation mechanisms are multiplicative and operate locally (say within a photoreceptor or midget bipolar cell) then long-term adaptation to a uniform bleaching field ought to have a very simple effect on spatial pattern vision. Specifically, a uniform bleaching field should effectively multiply the gain of each photoreceptor or bipolar cell by a scale factor that only depends upon the initial bleaching level and the elapsed time since offset of the bleaching field. If there is no other effect on the retinal circuitry (e.g. no changes in the relative strength of center and surround mechanisms) then long-term adaptation should be equivalent to scaling the intensity of input images by a factor that is independent of the spatial frequency content of the input. Therefore, the shape of the amplitude sensitivity function (amplitude sensitivity as a function of spatial frequency)* on a log sensitivity scale should be invariant during long-term dark adaptation. One aim of our experiments was to test this hypothesis.

Another aim was simply to obtain some systematic data on the changes in spatial pattern vision during long-term dark adaptation. Little is known about how detection thresholds for sinewave grating patterns (or any other patterns localized in spatial frequency) change during dark adaptation. One reason for this may be the difficulty of measuring grating thresholds during dark adaptation without introducing a background luminance which would affect the level and time course of adaptation. The problem is that sinewave gratings (and other stimuli localized in spatial frequency) must modulate in intensity above and below some mean level. We were able to circumvent this problem by using a new test pattern, which we call an *increment-Gabor* pattern—a Gaussian-damped sinewave summed with a simple Gaussian of the same amplitude (see Methods).

Background adaptation

Although the above prediction of shape-invariant amplitude sensitivity functions (ASFs) follows directly from previous studies of long-term dark adaptation, the prediction is somewhat surprising within the context of previous work in spatial pattern vision. It is well-known that the shape of the ASF (or equivalently the CSF) on a log sensitivity axis changes considerably as the background luminance level is changed (e.g. Kelly, 1972; Van Nes & Bouman, 1967). As background luminance increases, sensitivity at high spatial frequencies increases relative to sensitivity at low spatial frequencies, and the peak of the ASF shifts toward higher spatial frequencies. These changes in ASF shape correspond to the fact that *background-adaptation curves* (threshold as a function of adapting-background intensity) for low spatial frequencies follow Weber's law above the lowest background luminances, whereas the background-adaptation curves for high spatial frequencies follow the DeVries–Rose (square-root) law for a substantial range of intermediate background luminances before the transition to Weber's law (e.g. Kelly, 1972).

According to the *equivalent-background hypothesis*, the adaptation effects produced by bleaching are equivalent to those produced by a steady background (Crawford, 1947; Stiles & Crawford, 1932). There is some impressive evidence for this hypothesis in the rod system, and rather mixed evidence for the hypothesis in the cone system (for a review, see Hood & Finkelstein, 1986). If, in fact, background adaptation and bleaching adaptation have equivalent effects on spatial vision then one would expect them to have the same effect on the shape of the ASF. Given the context of the existing grating-detection literature, this prediction would seem to be at odds with predictions based upon the dark-adaptation studies described above.

*The amplitude sensitivity function (ASF) is closely related to the more familiar contrast sensitivity function (CSF). In the standard paradigm, contrast sensitivity is simply amplitude sensitivity multiplied by the background intensity. When the background is dark, as in some of the present experimental conditions, contrast sensitivity is not a useful quantity for describing the results (see Methods).

In order to test the equivalent-background hypothesis and in order to confirm the major findings of the grating-detection literature under our stimulus conditions (which use the new increment-Gabor target), we also measured ASFs as a function of background luminance.

METHODS

Subjects

Two subjects, a 42-yr-old male and a 25-yr-old male, participated in the experiment. Both subjects had 20/20 corrected Snellan acuity (or better) and normal color vision, as tested using Dvorine color plates. The subjects had full knowledge of the purpose of the experiment and were extensively practiced prior to any data collection.

Stimuli

A central aim of the present study was to measure amplitude sensitivity functions (ASFs) in the dark, following full bleaches, and in the light, on steady adapting backgrounds. In order to measure ASFs in the fovea, it is necessary to use targets that are localized both in spatial frequency and in space. The most common targets used to achieve this goal have been the Gaussian-damped sinewave grating (a Gabor target) or the high-order derivative of a Gaussian. While these targets are well-suited for measurements on steady adapting backgrounds, they are poorly suited for measurements in the dark because they require a background intensity around which to modulate. This background intensity might produce unwanted adaptation effects which contaminate the dark-adaptation measurements.

In order to circumvent this problem we used a briefly presented "increment-Gabor" target which consisted of a Gabor waveform summed with a simple Gaussian waveform of the same amplitude and space constant (standard deviation) as the Gabor waveform (Hahn & Geisler, 1991). The addition of the Gaussian had the desired effect of causing all modulation to be in the positive direction (with respect to the background).

The increment-Gabor pattern is defined by the equation:

$$I(x,y)=A\exp\left[-\frac{(x-x_0)^2+(y-y_0)^2}{2\sigma^2}\right]\times\{1+\sin(2\pi\mu[(x-x_0)\cos\theta+(y-y_0)\sin\theta])\} \quad (1)$$

where A is the amplitude, σ the standard deviation (spatial spread)*, μ the dominant spatial frequency, θ the orientation, and (x_0, y_0) the spatial location. Notice that this is a two-dimensional waveform that falls off with a Gaussian envelope in all directions. The left side of Fig. 1 shows the one-dimensional profile of the Gaussian component, the Gabor component, and the increment-Gabor target (the sum of the two components). The amplitude spectra (the square-root of the power spectra) of the these waveforms are plotted in the right side of Fig. 1.

As can be seen in Fig. 1C, there is significant energy in the increment-Gabor target at very low spatial frequencies due to the Gaussian component. This raises a potential difficulty: in a simple detection task the subject could base detection upon the low spatial frequency information in the Gaussian component, rather than on the spatial frequency information in the Gabor component. To eliminate this possibility we used a discrimination task in which the subject had to decide whether the increment-Gabor stimulus was oriented at $+45°$ (45° to the right) or $-45°$ (45° to the left). The thresholds measured using this task must be based solely upon the frequency content of the Gabor pattern because the frequency components due to the Gaussian pattern are identical for both target orientations.

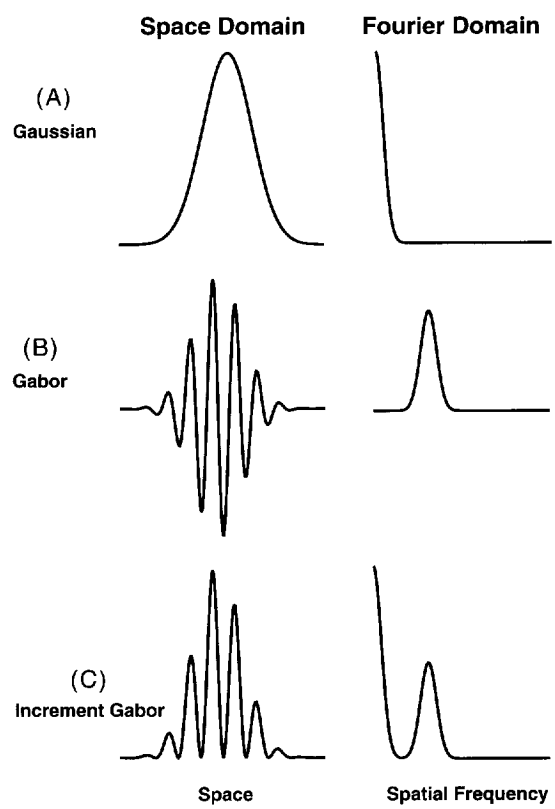

FIGURE 1. An increment-Gabor test pattern (0.5 octave bandwidth), and its subcomponents, illustrated in the space and Fourier domains. The increment-Gabor pattern (C) consists of the sum of a Gaussian pattern (A) and a Gabor pattern (B) of the same spatial width [see text equation (1)]. The left panel shows the intensity profiles, and the right panel the profiles of amplitude spectra (positive frequencies only). Note that the increment-Gabor pattern modulates entirely above the background, but contains low-frequency components. The actual test patterns were two-dimensional, with the same Gaussian envelope in all directions. To ensure that detection was based upon the frequency components of the Gabor sub-pattern, the subject was required to judge whether the pattern was titled 45° to the left or 45° to the right.

*The spatial extent (and hence bandwidth) of the target stimulus is determined by the standard deviation parameter of the Gaussian damping function,

$$\sigma=\frac{\sqrt{\ln(c)/2}}{\pi\mu}\frac{(2^\omega+1)}{(2^\omega-1)},$$

where μ is the center frequency, ω is the bandwidth, and c is the criterion height used to define bandwidth. In the present study the bandwidths were 0.5 octaves ($\omega=0.5$) at half height ($c=0.5$).

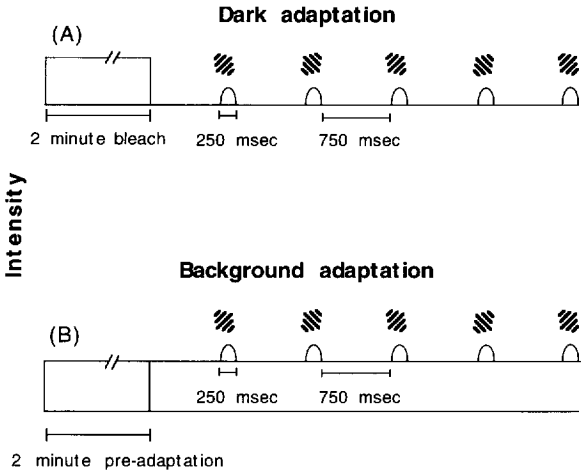

FIGURE 2. Stimulus presentation sequences used during dark adaptation (A) and during background adaptation (B). Following a full bleach, or following 2 min of adaptation to the adapting background (intensity $= I_b$), the increment-Gabor target (spatial frequency $= \mu$, amplitude $= A$) was presented for 250 msec once every second. The increment-Gabor target was ramped on and off with a Gaussian profile (temporal standard deviation = 83.33 msec). The orientation of the pattern alternated between $+45°$ and $-45°$.

In the discrimination task, the thresholds were measured by varying the amplitude, A, which is the amplitude of *both* the Gaussian and Gabor components. This maintains the Gaussian amplitude at the smallest value sufficient to keep the entire waveform above the background intensity (hence minimizing any light-adaptation effects of the test target). One consequence of using this target is that it is not useful to express threshold in terms of contrast [i.e., $C=(I_{max}-I_{min})/(I_{max}+I_{min})$], especially when the thresholds are measured against a dark background. This is because an increment-Gabor target presented in the dark always has a contrast of 1.0 independent of amplitude. The data are reported here as amplitude thresholds, or amplitude sensitivities, even when measurements were made against a background field.

Amplitude thresholds were measured during dark adaptation following 2 min of adaptation to a bleaching field of 5.77 log td, which bleached an estimated 97% of the photopigment (Rushton & Henry, 1968). Amplitude thresholds were also measured on steady adapting backgrounds of 0.46, 0.99, 1.6, 1.9, 2.5, 3, 3.6 and 4.1 log td. The increment-Gabor targets had dominant spatial frequencies of 1, 3, 7, 10 or 15 c/deg and a bandwidth of 0.5 octaves at half height. A single stimulus presentation had a duration of 250 msec, during which the amplitude was temporally ramped on and off with a Gaussian profile (temporal standard deviation of 83.33 msec). The two orientations of the increment-Gabor target ($+45°$ and $-45°$) were presented alternately, separated by 750 msec. A time line illustrating the temporal order of stimulus presentation is shown in Fig. 2.

Apparatus

The target stimuli were created on a PDP-11/73 computer with an ADAGE graphics processor, and displayed on a Tektronics SR690 color monitor which operated in a non-interlaced mode at 120 Hz. The range of stimulus sizes required that the monitor be located 215 cm from the subject for low frequencies (1 and 3 c/deg) and 700 cm for high frequencies (7, 10 and 15 c/deg).

The background and bleaching stimuli subtended 6.8° and were produced with a single channel of a Maxwellian-view system. The light source was a Sylvania tungsten halogen lamp (500 Q/CL). The retinal illumination of the bleaching and background fields were set using Kodak neutral density filters. The bleaching and background fields were switched on and off, under computer control, using an electromechanical shutter with a transition time of under 1 msec.

The target and background stimuli were combined with a beam-splitter cube and were viewed monocularly through a 3-mm artificial pupil placed just in front of the cornea. A bite-bar was used to stabilize head position.

Calibration

The luminances produced by the monitor were controlled by look-up tables in the ADAGE processor, which has 10-bit digital-to-analog converters. The calibration of the monitor was carried out as follows. First, a photometer was used to measure and set the maximum luminance. Second, the relative luminance was measured as a function of the output value in the look-up tables by reading the response of a United Detector Technologies (PIN 10AP) photodiode with a 12-bit analog-to-digital converter. The 1024 luminance measures were then fit with a smooth function (Cowan, 1983), and this function was used to create linear look-up tables with 256 entries. The amplitude of the increment-Gabor probe was controlled by adjusting the luminance range of the look-up table. Prior to each experimental session, the calibration of the monitor was checked by reading the response of the photodiode at two fixed look-up table values. The day-to-day variations in the measured luminances were negligible.

The retinal illuminances produced by the Maxwellian view channel were measured using the method of Westheimer (1966). The channel illuminances were set every day by monitoring the response of a photodiode placed at a known position just behind the artificial pupil. The stability of the light source was checked by comparing photodiode responses before and after each experimental session.

Procedure

In each experimental session, thresholds were measured during dark adaptation and against all background luminances, for a single spatial frequency, using the method of adjustment, which has been shown to produce results similar to forced-choice methods (Kelly & Savoie, 1973; Kortum & Geisler, 1995).

During the dark-adaptation phase of the experiment, thresholds were measured for 900 sec following offset of the bleaching field. The subject repeatedly adjusted the amplitude of the increment-Gabor target until discrimi-

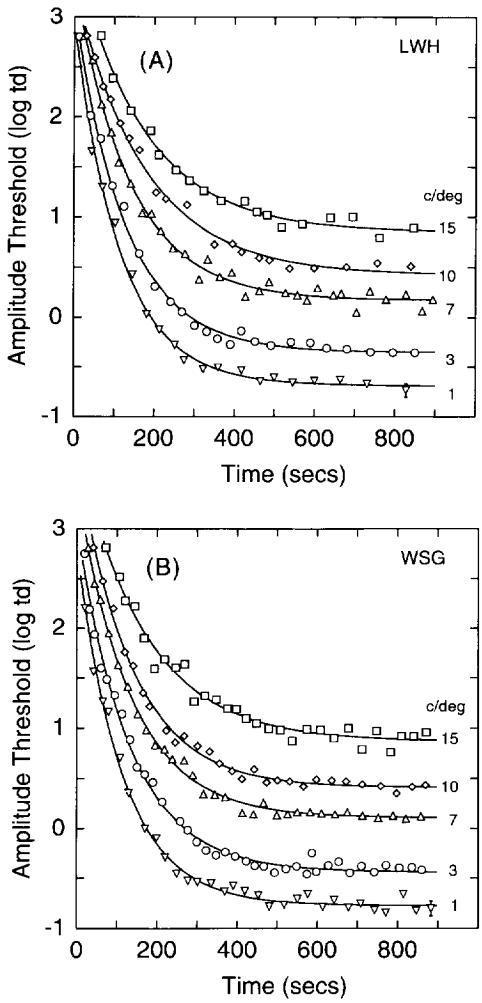

FIGURE 3. Dark-adaptation curves measured for the spatial frequencies indicated on the right. (A) Subject LWH. (B) Subject WSG. Each data point represents the average of three measurements. The error bar on the data point at the far right in the lowest curve indicates the average standard error (LWH 0.066 log td; WSG 0.075 log td). The solid curves are the best fit of a simple equation [see text equation (2)] used to interpolate the data.

nation between the two orientations was at threshold (which was signaled by a button press).

Following the measurements during dark adaptation, thresholds were measured on the steady backgrounds beginning at the lowest background intensity and working up to the highest background intensity. For each background intensity there was a 2-min light-adaptation period prior to making threshold adjustments. For some of the higher spatial frequencies, thresholds could not be measured at the highest background intensities because the threshold amplitudes exceeded the maximum that could be produced by the monitor.

*The three adjustment thresholds represented by each data point were in fact measured at slightly different times (because of the adjustment procedure). The points are plotted on the abscissa at the mean of the three different times.

†The solver options were set to use linear extrapolation from a tangent vector for estimating the initial parameters. The search method was quasi-Newtonian; forward differencing was used to estimate the partial derivatives. The precision of the calculations was set at 1.0 $\times 10^{-6}$.

RESULTS

The amplitude thresholds measured during dark-adaptation following the full bleach are shown in Fig. 3 for both subjects. The figure gives the logarithm of amplitude threshold as a function of time after the offset of the bleaching field for the spatial frequencies indicated on the right. In these plots, each point represents the mean of three threshold measurements*. The average standard error across all the data points is indicated by the error bars on the last data point of the 1 c/deg curve. The dark-adaptation curves for the different spatial frequency targets are similar in shape and time course, but are spread out systematically as a function of target spatial frequency—the higher the spatial frequency the higher the threshold.

For the purpose of summarizing the data and testing the equivalent-background hypothesis, each dark-adaptation curve was fit with an exponential decay function of the following form:

$$\log A(t) = \alpha e^{-t/t_0} + \beta, \quad (2)$$

where $A(t)$ is amplitude threshold at time t, β is the dark-adapted threshold (the lower asymptote), α is the initial increase in log threshold due to bleaching adaptation, and t_0 is the time constant of recovery. Equation (2) was fit to the data with the "solver" feature of Microsoft Excel 3.0, using a minimum-squared-error criterion†. The solid curves in Fig. 3 are the best-fitting functions. As can be seen, there were no systematic deviations between the data and the fitted functions.

The amplitude thresholds measured on steady adapting backgrounds are shown in Fig. 4 for the two subjects. The figure gives the logarithm of amplitude threshold as a function of adapting background intensity. Each plotted point represents the average of at least six threshold measurements. The average standard error across all the data points is indicated by the error bars on downward-pointing triangle at 0.46 log td. As can be seen, the background-adaptation curves systematically change position and shape, as a function of target spatial frequency. As spatial frequency increases, the background adaptation curves shift vertically; as background intensity increases, the curves converge (i.e. the vertical separation lessens). The convergence of the background adaptation curves is consistent with previous work (Kelly, 1972; Van Nes & Bouman, 1967). For low spatial frequencies, there is quick transition from a plateau of constant threshold to Weber's law (a slope of 1.0). For high spatial frequencies there is a more gradual transition.

For the purpose of summarizing the data and testing the equivalent-background hypothesis, each background-adaptation curve was fit with a function of the following form:

$$\log A(I_b) = 0.5 \log_{10}(I_b + \alpha) + 0.5 \log_{10}(I_b + \alpha + \beta) + \gamma, \quad (3)$$

where $A(I_b)$ is amplitude threshold for background

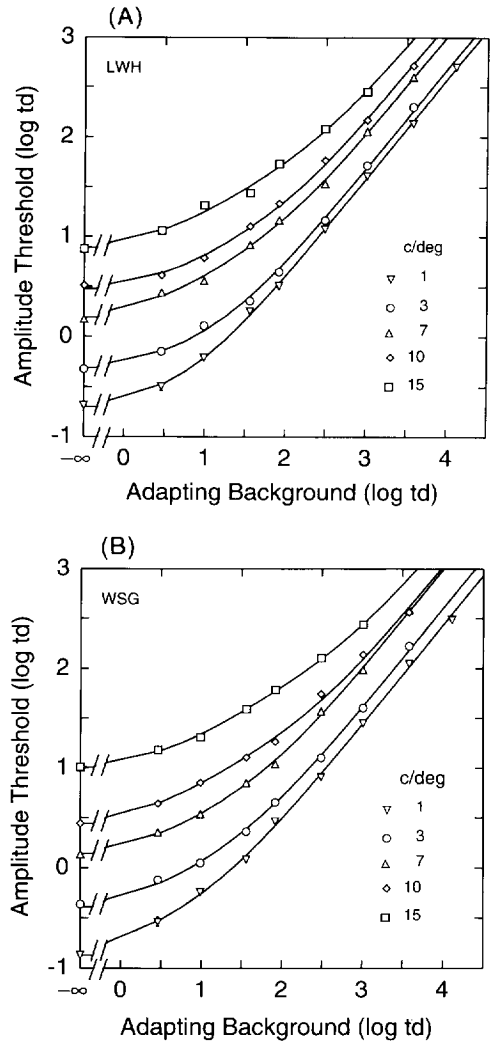

FIGURE 4. Background-adaptation curves measured for the spatial frequencies indicated on the right. (A) Subject LWH. (B) Subject WSG. Each data point represents the average of six measurements. The error bar on the data point at 0.46 log td in the lowest curve, indicates the average standard error (LWH 0.038 log td; WSG 0.046 log td). The solid curves are the best fit of a simple equation [see text equation (3)] used to interpolate the data.

intensity I_b, and α, β and γ are free parameters. This function was picked because it is capable of producing a smooth transition from a plateau region, to a square-root (De Vries–Rose) region, to a Weber region. [However, no particular theoretical significance should be attached to the individual terms in equation (3).] As before, this function was fit to the amplitude threshold data using the solver feature of Microsoft Excel 3.0. The solid curves in Fig. 4 are the best-fitting functions. Again, there do not appear to be any systematic deviations between the data and the fitted functions.

In order to more clearly see the effects of adaptation on spatial pattern detection, we replotted the data as amplitude sensitivity functions (ASFs, by taking vertical slices through the fitted dark-adaptation and background-adaptation curves at different times and at different background intensities, respectively. Note that amplitude sensitivity is defined to be one over the amplitude threshold ($1/A$).

Figure 5 shows the ASFs at six different points in time during dark adaptation. The thick solid curve shows the ASF obtained in the dark-adapted eye. As can be seen, the ASFs shift upward during dark adaptation, and all have a low-pass shape (i.e. they fall-off monotonically with increasing spatial frequency). To compare shapes, the ASFs were normalized to 1.0 at 1 c/deg and replotted. The result is shown in Fig. 6. This figure shows that the ASFs are nearly identical in shape throughout the course of long-term dark adaptation, with perhaps a slightly shallower high-frequency fall-off in the dark-adapted eye.

Figure 7 shows the ASFs at six different background adaptation intensities. Again the thick curve shows the ASF in the dark-adapted eye. The ASFs shift downward with increasing background adaptation, and all have a low-pass shape. The ASFs were normalized to 1.0 at 1 c/deg for the purpose of comparing shapes. The result is shown in Fig. 8. As can be seen, the ASFs change shape with background adaptation level; as the background intensity increases, the ASFs become flatter. This is completely different from the effect of bleaching

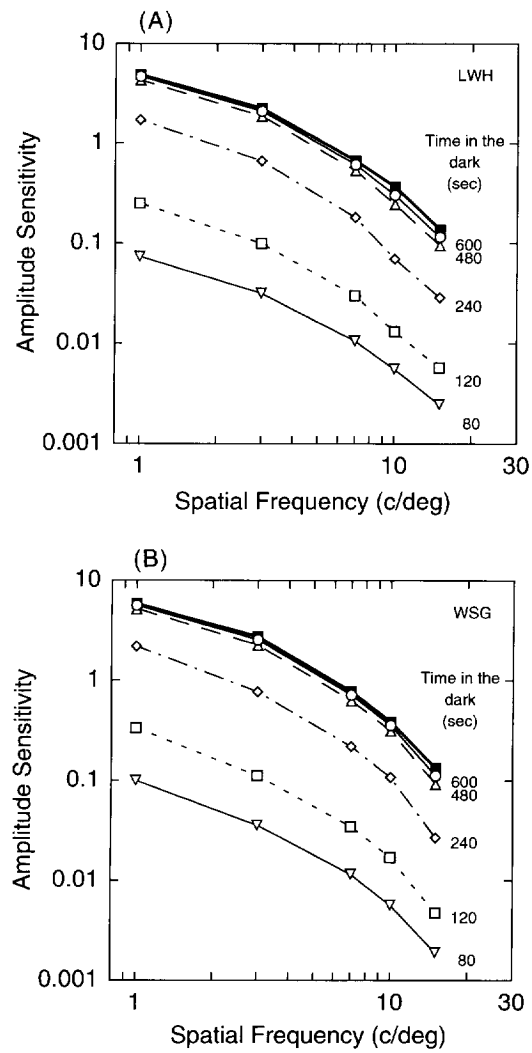

FIGURE 5. Amplitude sensitivity functions (1/amplitude-threshold as a function of spatial frequency) for the times during dark adaptation indicated on the right. These curves were derived from the solid curves in Fig. 3. (A) Subject LWH. (B) Subject WSG.

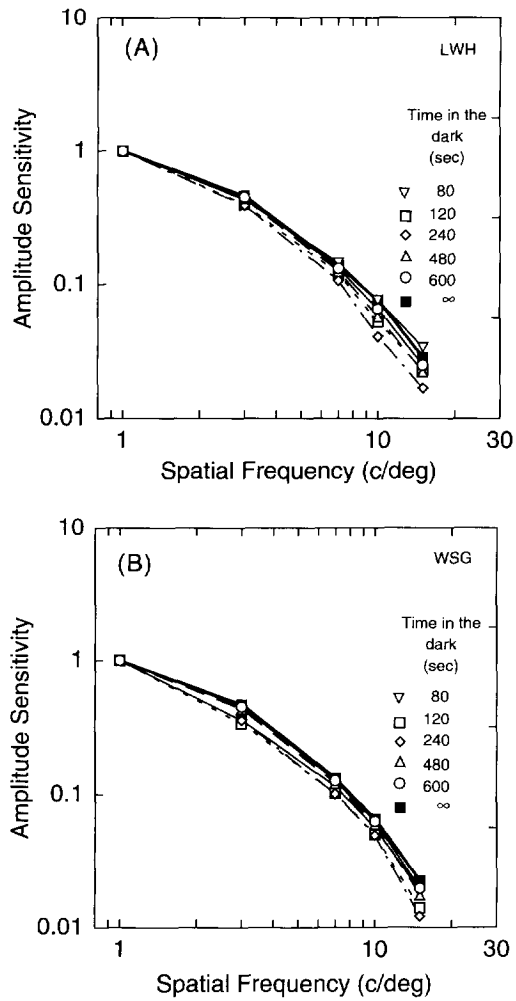

FIGURE 6. Amplitude sensitivity functions (1/amplitude-threshold as a function of spatial frequency) for the times during dark adaptation indicated on the right. These curves are identical to those in Fig. 5, except they have been normalized to a value of 1.0 at 1 c/deg (A) Subject LWH. (B) Subject WSG. Note that the normalized ASFs are nearly superimposed, indicating shape invariance during dark adaptation.

adaptation, where, if anything, the ASF in the dark-adapted eye is slightly shallower than in the light-adapted eye.

DISCUSSION

A major goal of the present study was to measure, for the first time, spatial pattern detection performance for sinewave grating targets during long-term dark adaptation. We found that the dark adaptation curves were parallel for targets ranging from 1 to 15 c/deg, or equivalently, that the amplitude sensitivity functions (ASFs) were identical in shape throughout the course of long-term dark adaptation. A very different result was obtained when detection performance was measured on adapting backgrounds for a broad range of background intensity levels. We found, in agreement with earlier work, that the background-adaptation curves for different spatial frequencies converged as background intensity increased, or equivalently, that the ASFs changed shape (becoming flatter) as background intensity increased.

All of the measured amplitude sensitivity functions were low-pass in shape (i.e., there was no low-frequency fall-off). Although this result violates the typical textbook description of the contrast-sensitivity function (CSF), it is generally consistent with the literature. First, the magnitude of the low-frequency fall off has been found to be greatly reduced for brief presentations of the target grating (Nachmias, 1967; Arend, 1976; Robson & Graham, 1981), or when grating contrast is temporally modulated at frequencies above a couple of cycles per second (Robson, 1966). The gratings in the present experiment were presented for 250 msec, a relatively short duration. Second, the magnitude of the low-frequency fall-off has been found to be less pronounced when the target gratings contain a fixed number of cycles (e.g. Banks, Geisler & Bennett, 1987; Robson & Graham, 1981). The gratings in the present experiment were 0.5 octaves in bandwidth and hence contained a fixed number of cycles.

The absence of a low-frequency fall-off does not imply an absence of spatially antagonistic receptive-field properties. Several studies have shown that for the

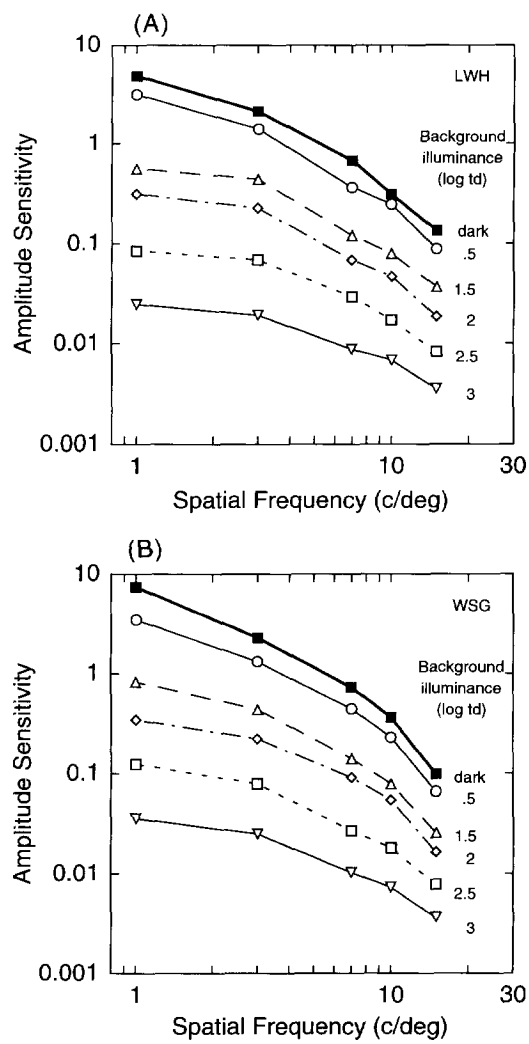

FIGURE 7. Amplitude sensitivity functions (1/amplitude-threshold as a function of spatial frequency) for the background adaptation intensities indicated on the right. These curves were derived from the solid curves in Fig. 4. (A) Subject LWH. (B) Subject WSG.

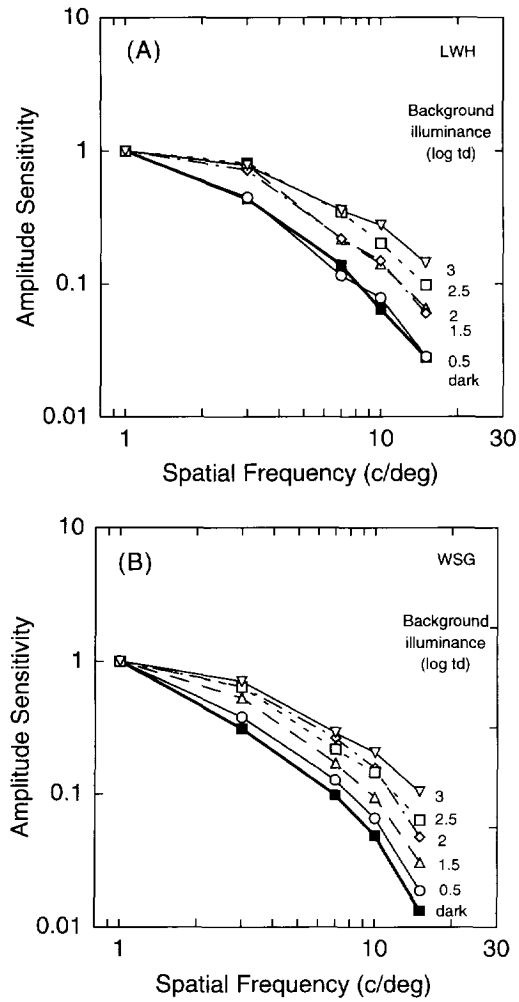

FIGURE 8. Amplitude sensitivity functions (1/amplitude-threshold as a function of spatial frequency) for the background adaptation intensities indicated on the right. These curves are identical to those in Fig. 7, except they have been normalized to a value of 1.0 at 1 c/deg. (A) Subject LWH. (B) Subject WSG. Note that the normalized ASFs do not superimpose, indicating a lack of shape invariance across background adaptation levels. The ASFs become progressively flatter as adapting background intensity increases.

detection of sinewave gratings, the photopic visual system appears to sum over approximately a fixed number of spatial cycles (e.g. Banks, Sekuler & Anderson, 1991; Howell & Hess, 1978). Furthermore, it can be shown that if visual performance were only limited by photon noise and by this fixed-cycle-summation property, then the ASF (or CSF) would be monotonically decreasing with a slope of -1 in log–log coordinates (Banks *et al.*, 1987). The fact that the present ASFs have a slope considerably less than 1.0 at low spatial frequencies may be due to spatially antagonistic receptive-field properties (for more discussion, see Geisler & Banks, 1994).

Equivalent-background hypothesis

In the 1930s, Stiles and Crawford introduced the hypothesis that bleaching and background adaptation might be equivalent, in the sense that for each point in time during dark adaptation there might be a unique background intensity which affects the visual system in an identical fashion (Crawford, 1947; Stiles & Crawford, 1932). If the hypothesis is correct, then measurements of performance in the presence of adapting backgrounds can be used to predict performance during dark adaptation (which, in general, is more difficult to measure). They showed that the equivalent-background hypothesis can be tested by first finding a background intensity and a point in time during dark adaptation that produces the same threshold for the same target. If the equivalent-background hypothesis is correct then thresholds should remain equated for any change in the target.

The fact that the ASFs were found to be constant in shape during dark adaptation and to change shape as a function of adapting-background intensity is strong evidence against the equivalent-background hypothesis (at least for the domain of spatial pattern vision). This failure of the equivalent-background hypothesis is illustrated in Fig. 9, which replots the dark-adaptation and background-adaptation curves (for subject LWH) from Figs 3 and 4. The four vertical line segments in the figure are all identical in length. Recall that the upper curve in both figures is for the 15 c/deg target. Comparison of the upper line segments in the two figures shows that a background of approx. 3 log td produces the same threshold for a 15 c/deg target as a point in time after the bleach of 80 sec. Contrary to the equivalent-background hypothesis, the thresholds are not equal for the 1 c/deg target (the bottom curves). If the equivalent-background hypothesis were correct the upper right line segment would just cover the five curves.

The failure of the equivalent-background hypothesis for variations in target spatial frequency is consistent with the failures found in probe-flash experiments (Geisler, 1981). Geisler (1979) found little evidence against the equivalent-background hypothesis for spot targets of varying diameter, but as Hood and Finklestein (1986) note, the small variations in the shapes of the background-adaptation curves with spot diameter weakened the strength of the test. Thus, it seems safe to conclude that the equivalent-background hypothesis (for bleaching and background adaptation in the cone system) can be put to rest.

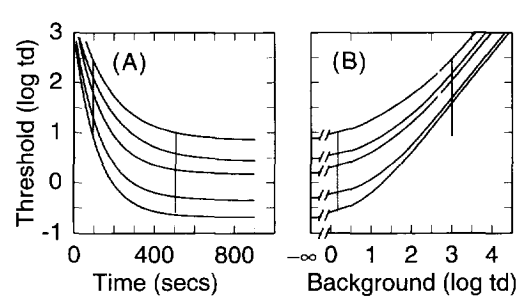

FIGURE 9. Illustration of the failure of the equivalent-background hypothesis. The curves in A are the dark-adaptation curves from Fig. 3A. The curves in B are the background-adaptation curves from Fig. 4A. The four vertical line segments are all of identical length. If the equivalent-background hypothesis were correct the upper line segment in the right panel would just cover the five curves.

Mechanisms of bleaching adaptation

As described in the Introduction, there is evidence that long-term (bleaching) adaptation in the fovea is both local (Cicerone *et al.*, 1990; MacLeod & Hayhoe, 1976), and multiplicative (Geisler, 1981). If bleaching adaptation is local and multiplicative then a uniform bleaching field ought to effectively scale all receptor locations within the field by a multiplicative gain factor. The effect on performance would be to shift the ASF vertically on a log–log axis, without affecting shape. On the other hand, if bleaching adaptation were to affect the size of spatial pooling regions or the balance between antagonistic regions within visual receptive fields (these are examples of non-local adaptation) then there would not only be vertical shifts of the amplitude sensitivity functions, but changes in shape. As shown in Fig. 6, we found essentially no change in the shape of the ASF.

It is important to note that not all forms of non-local adaptation can be detected by measuring ASFs for uniform bleaching fields. For example, reductions in gain produced by pooling over receptor or bipolar responses would leave the shape of the ASF invariant, as long as there were no changes in the size of spatial pooling or the balance of antagonistic receptive-field regions. Similarly, the invariance of ASF shape does not imply multiplicative adaptation. For example, local subtractive adaptation could also produce shape invariance. However, when the results of the current and previous cone dark-adaptation studies are considered as a whole, they point to a simple model of long-term bleaching adaptation in which the adaptation is both local and multiplicative.

Although the long-term adaptation mechanisms have a simple multiplicative effect in the present experiments, the way in which they are implemented within the visual system is likely to be rather complex. To begin with, long-term multiplicative adaptation must have at least two components: photopigment depletion and a neural component. Photopigment depletion behaves simply, like a variable density filter, but is too weak to account for more than a modest fraction of the threshold elevation (e.g. see Geisler, 1978a). The long-term neural adaptation mechanism does not behave like a variable density filter; rather, it appears to have complex effects on temporal processing. For example, Hayhoe and Chen (1986) found that short- and long-duration bleaches have different effects on the temporal contrast sensitivity measured during long-term dark adaptation.

Mechanisms of background adaptation

The fact that the shape of the amplitude sensitivity function changes substantially with background adaptation intensity suggests that the mechanisms of background adaptation are not entirely local and therefore must be different from those of bleaching adaptation. However, it must be the case that some of the adaptation effects produced by steady backgrounds are due to the bleaching adaptation mechanisms. In this sense, background adaptation is likely to be more complex than bleaching adaptation. The next paper in this series examines the effects of background adaptation on spatial pattern detection using the probe-flash paradigm (Kortum & Geisler, 1995).

REFERENCES

Arend, L. E. Jr. (1976). Temporal determinants of the form of the spatial contrast threshold MTF. *Vision Research*, *16*, 1035–1042.

Banks, M. S., Geisler, W. S. & Bennett, P. J. (1987). The physical limits of grating visibility. *Vision Research*, *27*, 1915–1924.

Banks, M. S., Sekuler, A. B. & Anderson, S. J. (1991). Peripheral spatial vision: Limits imposed by optics, photoreceptors, and receptor pooling. *Journal of the Optical Society of America*, *8*, 1775–1787.

Brindley, G. S. (1962). Two new properties of foveal after-images and a photochemical hypothesis to explain them. *Journal of Physiology*, *164*, 168–179.

Cicerone, C. M., Hayhoe, M. M. & MacLeod, D. I. A. (1990). The spread of adaptation in human foveal and parafoveal cone vision. *Vision Research*, *30*(11), 1603–1615.

Cowan, W. B. (1983). An inexpensive scheme for calibration of a colour monitor in terms of CIE standard coordinates. *Computer Graphics*, *17*, 315–321.

Crawford, B. H. (1947). Visual adaptation in relation to brief conditioning stimuli. *Proceedings of the Royal Society of London Series B*, *134*, 283–103.

Geisler, W. S. (1978a). Effects of photopigment depletion on brightness and threshold. *Vision Research*, *18*, 269–278.

Geisler, W. S. (1978b). Adaptation, afterimages and cone saturation. *Vision Research*, *18*, 279–289.

Geisler, W. S. (1979). Initial-image and afterimage discrimination in the human rod and cone systems. *Journal of Physiology*, *London*, *294*, 165–179.

Geisler, W. S. (1981). Effects of bleaching and backgrounds on the flash response of the visual system. *Journal of Physiology*, *London*, *312*, 413–434.

Geisler, W. S. (1983). Mechanisms of visual sensitivity: Backgrounds and early dark adaptation. *Vision Research*, *23*, 1423–1432.

Geisler, W. S. & Banks, M. S. (1994). Visual Performance. In Bass, M. (Ed.), *Handbook of optics* (2nd edn, Vol. 1). New York: McGraw-Hill.

Hahn, L. W. & Geisler, W. S. (1991). Contrast sensitivity functions measured during dark adaptation and on steady backgrounds, in *OSA Annual Meeting Technical Digest*, *1991* (Optical Society of America, Washington, DC, 1991), Vol. 17, pp. 164.

Hayhoe, M. M. (1990). Spatial interactions and models of adaptation. *Vision Research*, *30*(6), 957–965.

Hayhoe, M. M. & Chen, B. (1986). Temporal modulation sensitivity during cone dark adaptation. *Vision Research*, *26*, 1715–1725.

Hayhoe, M. M. & Smith, M. V. (1989). The role of spatial filtering in sensitivity regulation. *Vision Research*, *28*(4), 457–469.

Hood, D. C. & Finkelstein, M. A. (1986). Sensitivity to light. In K. R. Boff, L. Kaufman & J. P. Thomas (Eds.), *Handbook of perception and human performance*. New York: John Wiley and Sons.

Hood, D. C., Ilves, T., Mauer, E., Wandell, B. & Buckingham, E. (1978). Human cone saturation as a function of ambient intensity: A test of models of shifts in the dynamic range. *Vision Research*, *19*, 983–993.

Howell, E. R. & Hess, R. F. (1978). The functional area for summation to threshold for sinusoidal gratings. *Vision Research*, *18*, 369–374.

Kelly, D. H. (1972). Adaptation effects on spatio-temporal sine-wave thresholds. *Vision Research*, *12*, 89–101.

Kelly, D. H. & Savoie, H. E. (1973). A study of sine-wave contrast sensitivity by two psychophysical methods. *Perception and Psychophysics*, *14*, 313–318.

Kortum, P. T. & Geisler, W. S. (1995). Adaptation mechanisms in spatial vision—II. Flash thresholds and background adaptation. *Vision Research*, *35*, 1595–1609.

MacLeod, D. I. A. & Hayhoe, M. M. (1976). Retention of detail in afterimages: Sharply localized sensitivity loss in the fovea. *Proceedings of the Association for Research in Vision and Ophthalmology*, 82.

Nachmias, J. (1967) Effect of exposure duration on visual contrast

sensitivity with square-wave gratings. *Journal of the Optical Society of America*, *57*, 421–427.

Robson, J. G. (1966). Spatial and temporal contrast sensitivity functions of the visual system. *Journal of the Optical Society of America*, *56*, 1141–1142.

Robson, J. G. & Graham, N. (1981). Probability summation and regional variation in contrast sensitivity across the visual field. *Vision Research*, *21*, 409–418.

Rushton, W. A. H. & Henry, G. H. (1968). Bleaching and regeneration of cone pigments in man. *Vision Research*, *8*, 617–631Y

Rushton, W. A. H. & Westheimer, G. (1962). The effect upon the rod threshold of bleaching neighboring rods. *Journal of Physiology*, *164*, 318–329.

Shapley, R. & Enroth-Cugell, C. (1984). Visual adaptation and retinal gain controls. *Progress in Retinal Research*, *3*, 263–346.

Stiles, W. S. & Crawford, B. H. (1932). Equivalent adaptation levels in localized retinal areas. *Rep. Discussion Vision. Physical Society (London)*, *194*.

Van Nes, F. L. & Bouman, M. A. (1967). Spatial modulation transfer in the human eye. *Journal of the Optical Society of America*, *57*, 401–406.

Walraven, J., Enroth-Cugell, C., Hood, D. C., MacLeod, D. I. A. & Schnapf, J. L. (1990). The control of visual sensitivity: Receptoral and postreceptoral processes. In Spillman, L. & Werner, J. S. (Eds.), *Visual perception: The neurophysiological foundations*. San Diego: Academic Press.

Westheimer, G. (1966). The Maxwellian view. *Vision Research*, *6*, 669–682.

Acknowledgements—This research was supported by NIH grant EY02688 and AFOSR grant F49620-93-1-0307 to WSG.